Behavior of the giant-dipole resonance in ^{120}Sn and ^{208}Pb at high excitation energy

W.E. Ormand[a,b], P.F. Bortignon[a], R.A. Broglia[a,c], and A. Bracco[a]

[a] *Dipartimento di Fisica, Università Degli Studi di Milano, and Istituto Nazionale di Fisica Nucleare, Sezione di Milano, Via Celoria 16, 20133 Milano, Italy*

[b] *Physics Division, Oak Ridge National Laboratory, P.O. Box 2008, MS-6373, Oak Ridge, TN 37831-6373 USA*

[c] *The Niels Bohr Institute, University of Copenhagen, Blegdamsvej 17, DK-2100 Copenhagen Ø, Denmark*

Abstract

The properties of the giant-dipole resonance (GDR) are calculated as a function of excitation energy, angular momentum, and the compound nucleus particle decay width in the nuclei ^{120}Sn and ^{208}Pb, and are compared with recent experimental data. Differences observed in the behavior of the full-width-at-half-maximum of the GDR for ^{120}Sn and ^{208}Pb are attributed to the fact that shell corrections in ^{208}Pb are stronger than in ^{120}Sn, and favor the spherical shape at low temperatures. The effects shell corrections have on both the free energy and the moments of inertia are discussed in detail. At high temperature, the FWHM in ^{120}Sn exhibits effects due to the evaporation width of the compound nucleus, while these effects are predicted for ^{208}Pb.

PACS number: 24.30.Cz

Typeset using REVTEX

I. INTRODUCTION

The study of the properties of the giant-dipole resonance (GDR) at finite intrinsic excitation energy has been the objective of many experimental programs during the past decade (see the reviews in Ref. [1]). These experiments yield important information regarding nuclear motion as a function of temperature. In particular, the role played by quantal and thermal fluctuations in the damping of the giant vibrations. In this connection, one can individualize the following central issues: (1) the temperature dependence of the intrinsic width [2,3]; (2) the time scale for thermal fluctuations testing the validity of either the adiabatic picture [4,6,5] or the occurrence of motional narrowing [7,8]; (3) the existence of a limiting temperature for the observation of collective motion in nuclei [10,9]; and (4) the influence of the lifetime of the compound nucleus on the observed width of the GDR [11]. Of particular importance to address these issues is a systematic and comprehensive comparison between experiment and theory over a wide range of temperatures for several nuclei.

One of the principal experimental techniques for observing the GDR in hot nuclei has been compound-nuclear reactions induced in heavy-ion collisions [1]. For the most part, the wide range of experiments performed so far indicate that the full-width-at-half-maximum (FWHM) of the GDR strength function increases as a function of temperature as is predicted by theories for the GDR in hot nuclei that account for adiabatic, large-amplitude thermal fluctuations of the nuclear shape [4,6,5]. Many of these experiments, however, involve slightly different compound systems and are often analyzed using different parameters – most notably the level-density parameter. In addition, because of the dynamics of heavy-ion collisions, the compound system is generally formed at high angular momentum. Indeed, those systems corresponding to the highest excitation energy typically have the largest angular momentum content. As such, it is difficult to separate the effects due to large-amplitude thermal fluctuations of the shape from those due to angular momentum.

Recently, two experimental methods for studying the effects of excitation energy and angular momentum separately on the GDR have been introduced. In experiments involving

compound nuclear reactions, large arrays of gamma detectors have been used in order to identify GDR photons associated with a system of definite angular momentum. With this experimental setup, the GDR may be studied within an angular momentum window that is usually of the order 10-15 units of angular momentum wide, and centered between 30-50 $\hbar$ [12]. An alternative technique is to excite a target nucleus by inelastic scattering with light particles [13], which, because of the light mass of the projectile, yields an excited system with a fairly small angular momentum. By comparing data from these experiments with theoretical predictions, it is now possible to analyze the GDR in hot nuclei in terms of the effects due to thermal fluctuations and angular momentum separately.

In an earlier letter [14], we presented the results of a systematic study of the FWHM for the giant-dipole resonance as a function of temperature, angular momentum, and intrinsic width for the nuclei ^{120}Sn and ^{208}Pb in comparison with recent experimental data from inelastic alpha scattering [13]. In this work, in addition to providing the details of how this study was carried out, we also expand upon that work by providing a prediction for the influence of the evaporation particles on the FWHM in ^{208}Pb at finite temperature. Because of the systematic analysis over a range of temperatures and the relatively low angular momentum of the emitting system, it is possible to draw conclusions regarding the separate roles played by shell corrections, angular momentum, and the lifetime of the compound nucleus on the observed width of the GDR.

This work is organized in the following manner. In section II, the formalism for calculating the effects of thermal fluctuations of the nuclear shape while projecting angular momentum is outlined. A model for the GDR utilizing a quantal, rotating harmonic oscillator is given in Section III. A description of the shell corrections to the free energy and moments of inertia is presented in Section IV, while results and conclusions are given in Sections V and VI, respectively.

II. THERMAL FLUCTUATIONS

The description of the GDR in hot nuclei begins by noting that at a finite temperature, T, large-amplitude thermal fluctuations of the nuclear shape play an important role in the observation of nuclear properties. Under the assumption that the time scale associated with thermal fluctuations is slow compared to the shift in the dipole frequency caused by the fluctuations (adiabatic motion), the GDR cross section consists of a weighted average over all shapes and orientations. Projecting angular momentum, J, the GDR cross section is evaluated via [15,16]

$$\sigma(E) = Z_J^{-1} \int \frac{\mathcal{D}[\alpha]}{\mathcal{I}(\beta,\gamma,\theta,\psi)^{3/2}} \sigma(\alpha,\omega_J;E) \mathrm{e}^{-F(T,\alpha,J)/T}, \quad (1)$$

where E is the photon energy, $\mathcal{D}[\alpha] = \beta^4 d\beta \sin(3\gamma) d\gamma \sin\theta d\theta d\phi d\psi$ is the volume element, with α denoting the deformation paramters β and γ and the Euler angles ϕ, θ, and ψ, and $Z_J = \int \mathcal{D}[\alpha]/\mathcal{I}^{3/2}\mathrm{e}^{-F/T}$. The factor $\mathcal{I}(\beta,\gamma,\theta,\psi)$ is given by

$$\mathcal{I}(\beta,\gamma,\theta,\psi) = I_1 \cos^2\psi \sin^2\theta + I_2 \sin^2\psi \sin^2\theta + I_3 \cos^2\theta, \quad (2)$$

where the I_k represent the deformation-dependent principal moments of inertia. The free energy is given by

$$F(T,\alpha,J) = F(T,\alpha,\omega_{rot}=0) + (J+1/2)^2/2\mathcal{I}(\beta,\gamma,\theta,\psi), \quad (3)$$

where $F(T,\alpha,\omega_{rot}=0)$ is the free energy evaluated in the cranking approximation with rotational frequency, ω_{rot}, equal to zero.

In many previous works [4,6,5], a different procedure involving a fixed rotational frequency method for projecting angular momentum has been used. In this formalism, Eq. (1) would be replaced by

$$\sigma(E) = Z_\omega^{-1} \int \mathcal{D}[\alpha] \sigma(\alpha,\omega;E) \mathrm{e}^{-F(T,\alpha,\omega)/T}, \quad (4)$$

where $Z_\omega = \int \mathcal{D}[\alpha]\mathrm{e}^{-F/T}$ and the free energy is given by

$$F(T,\alpha,\omega) = F(T,\alpha,\omega_{rot}=0) - \frac{1}{2}\mathcal{I}(\beta,\gamma,\theta,\psi)\omega^2. \tag{5}$$

In this scheme, the rotational frequency is determined such that the average angular momentum of the system is given by [15,16]

$$\langle J\rangle = J + 1/2 = T\frac{\partial}{\partial\omega}\ln Z_\omega = Z_\omega^{-1}\omega\int \mathcal{D}[\alpha]\mathcal{I}(\beta,\gamma,\theta,\psi)\mathrm{e}^{-F(T,\alpha,\omega)/T}. \tag{6}$$

The primary disadvantages of the fixed rotational frequency approach are that angular momentum is projected only on average and that for finite angular momentum the nuclear free energy in Eq. (5) exhibits a saddle point beyond which the system is unstable. This is illustrated in Fig. 1, where, in the lower panel, the free energy for ^{106}Sn is plotted along the oblate noncollective and prolate collective axes at a temperature of 2 MeV and a rotational frequency of 1.25 MeV, which corresponds to an average angular momentum of approximately $55\hbar$. The free energies were computed as described in Section IV, and effectively consist of only the liquid-drop component. In the upper panel of Fig. 1, the Boltzman weight factor $\exp[-(F - F_{eq})/T]$, where F_{eq} is the minimum of the free energy below the saddle point, is also plotted. From the figure, it is clear that at high temperature and high angular momentum, the presence of the saddle point can be a serious drawback, as it is not possible to perform the thermal averaging. In addition, an important shape transition occurring at high spin, known as the Jacobi transition, which is characterized by the sudden evolution from an oblate noncollective shape to a prolate collective shape with large deformation, is absent. The formalism of Eq. (1) was introduced in Ref. [15] to account for these deficiencies and to permit a description of the GDR at very high spin.

In Ref. [16], an additional method, where only the z- component of the angular momentum is projected is also presented. In this case, Eq. (1) is modified to

$$\sigma(E) = Z_{J_z}^{-1}\int \frac{\mathcal{D}[\alpha]}{\mathcal{I}(\beta,\gamma,\theta,\psi)^{1/2}}\sigma(\alpha,\omega_{J_z};E)\mathrm{e}^{-F(T,\alpha,J_z)/T}, \tag{7}$$

where $Z_{J_z} = \int \mathcal{D}[\alpha]/\mathcal{I}^{1/2}\mathrm{e}^{-F/T}$ and the free energy is given by

$$F(T,\alpha,J_z) = F(T,\alpha,\omega_{rot}=0) + (J_z)^2/2\mathcal{I}(\beta,\gamma,\theta,\psi). \tag{8}$$

The principle feature of this projection method is to give a better overall description than Eq. (1) for nonscalar observables such as the angular distribution a_2 coefficient, which is defined by

$$\sigma(E,\theta) = \sigma(E)[1 + a_2(E)P_2(\cos\theta)], \tag{9}$$

where θ is the angle between the observed gamma-ray and the polarized spin direction. In heavy-ion fusion experiments, $J \approx J_z$ and lies in a plane perpendicular to the beam direction, and θ is measured relative to the incident beam direction. Then, a_2 may be written in terms spherical tensor components σ_μ of the GDR cross section via

$$a_2(E) = \frac{1}{\sigma(E)}\left[\sigma_0(E) - \frac{1}{2}(\sigma_1(E) + \sigma_{-1}(E))\right], \tag{10}$$

with $\sigma = \sum_\mu \sigma_\mu$.

Here, we have performed calculations at low spin using all three methods of angular momentum projection, and find that for the FWHM all three methods give the same value to within a few hundred keV, with Eqs. (4) and (1) giving the largest and smallest, respectively. At much higher spins, $J \approx 50\hbar$, however, Eqs. (1) and (4) yield very different results because of the presence of the saddle-point barrier in the fixed rotational frequency scheme that does not account for the Jacobi transition, and limits the effect of thermal fluctuations. These issues are discussed in further detail in Ref. [16].

III. MODEL FOR THE GDR

In principle, the most appropriate description of the GDR strength function in a hot, rotating nucleus would be obtained by performing random phase approximation (RPA) calculations for each deformation and orientation. Because of the large number of points required in performing the thermal averaging of Eqs. (1), (4), and (7), however, this procedure is computationally impractical. Instead, we make use of the fact that RPA calculations indicate that the GDR is a strongly collective excitation that is also rather stable with temperature [17]. As such, for all practical purposes, the GDR may be modeled by a harmonic

vibration along the three principal nuclear axes with frequencies inversely proportional to the radius of each axis [18]. Variations of this approach (with both quantal and classical oscillators), have been used in the past [4,6,5,7,8], and for completeness, we describe in detail the model used in this work in the present section.

A harmonic oscillator description of the GDR may be derived from a many-body nuclear Hamiltonian H with a pure harmonic-oscillator single-particle potential and an isovector dipole-dipole interaction as the only two-body term [19,18]. For the general triaxial nucleus, we have

$$H = \frac{1}{2}\sum_{k=1}^{3}\left[\sum_{i=1}^{A}\left(P_k^2 + M\bar{\omega}_k^2 X_k^2\right)_i + \kappa_k\left(\sum_{i=1}^{A}(\tau_z X_k)_i\right)^2\right], \tag{11}$$

where τ_z is the third component of the isospin, the oscillator frequencies $\bar{\omega}_k$ are inversely proportional to the radius along the axis $k = 1, 2, 3$, with

$$\omega_0 = (\bar{\omega}_1\bar{\omega}_2\bar{\omega}_3)^{1/3} \approx 40A^{-1/3}\ \text{MeV}, \tag{12}$$

($\hbar = 1$), and κ_k is the dipole-dipole strength, which empirically is of the order $3M\omega_k^2/A$.

In Eq. (11), it is possible to introduce a canonical transformation in which H is split into two parts. The first describing the intrinsic nuclear degrees of freedom, while the second the collective GDR mode, which may be written as

$$H_D = \frac{1}{2}\sum_k\left(p_k^2 + E_k^2 d_k^2\right), \tag{13}$$

where d_k is the giant-dipole operator and p_k is the conjugate momentum. Using the Hill-Wheeler convention [20], the GDR resonance energies along the three intrinsic axes are [19]

$$E_k = E_0\frac{R_0}{R_k} = E_0 \exp\left[-\sqrt{\frac{5}{4\pi}}\beta\cos\left(\gamma + \frac{2\pi k}{3}\right)\right], \tag{14}$$

where $E_0 \approx 80A^{-1/3}$ MeV is the dipole energy for the spherical shape.

If the intrinsic nuclear frame is rotating with angular velocity $\vec{\omega}$, Eq. (13) must be modified to include the coriolis and centrifugal forces, becoming

$$H_D = \tfrac{1}{2}\sum_k (p_k^2 + E_k^2 d_k^2) - \vec{\omega}\cdot(\vec{d}\times\vec{p}), \tag{15}$$

where $\vec{\omega}$ may be taken along the z-axis in the external, fixed reference frame, and while projecting angular momentum is taken to be the saddle-point value $\omega_J = (J+1/2)/\mathcal{I}(\beta,\gamma,\theta,\psi)$, i.e., the frequency that maximizes the exponential factors in the projection integral [15,16]. In terms of creation and annihilation operators $a_k^\dagger$ and a_k, Eq. (15) may be written as

$$H_D = \tfrac{1}{2}\sum_k E_k(a_k^\dagger a_k + a_k a_k^\dagger) + \frac{i}{2}\sum_{ijk}\epsilon_{ijk}\omega_i\sqrt{\frac{E_k}{E_j}}\left[a_j^\dagger a_k^\dagger - a_j^\dagger a_k + a_j a_k^\dagger - a_j a_k\right]. \tag{16}$$

Consolidating the notation, we may write H_D as

$$H_D = \tfrac{1}{2}\sum_{jk}\left(A_{jk}a_j^\dagger a_k + A_{jk}^* a_k a_j^\dagger + B_{jk}a_j^\dagger a_k^\dagger + B_{jk}^* a_j a_k\right) \tag{17}$$

with

$$B_{jk} = i\epsilon_{ijk}\omega_i\frac{E_j - E_k}{2\sqrt{E_j E_k}} \tag{18}$$

and

$$A_{jk} = \begin{cases} E_j, & \text{if } j = k; \\ i\omega_i\frac{E_j+E_k}{2\sqrt{E_jE_k}}, & \text{if } i\neq j\neq k. \end{cases} \tag{19}$$

At this point, we note that H_D is only a quadratic function of the coordinates, and, therefore, it is possible to introduce a canonical transformation

$$O_\nu^\dagger = \sum_k\left(X_k^\nu a_k^\dagger - Y_k^\nu a_k\right), \tag{20}$$

$$O_\nu = \sum_k\left(X_k^{\nu *} a_k^\dagger - Y_k^{\nu *} a_k\right), \tag{21}$$

such that the Hamiltonian may be written as

$$H_D = \tfrac{1}{2}\sum_\nu E_\nu\left(O_\nu^\dagger O_\nu + O_\nu O_\nu^\dagger\right). \tag{22}$$

The eigenenergies and transformation coefficients X and Y are found from the 6×6 RPA-like eigenvalue problem

$$\begin{pmatrix} A & B \\ A^* & B^* \end{pmatrix}\begin{pmatrix} X^\nu \\ Y^\nu \end{pmatrix} = E_\nu\begin{pmatrix} 1 & 0 \\ 0 & -1 \end{pmatrix}\begin{pmatrix} X^\nu \\ Y^\nu \end{pmatrix}. \tag{23}$$

Note that the eigenvalues E_ν come in plus-minus pairs, and the three principal modes of the GDR correspond to the three positive eigenvalues.

In order to evaluate the GDR photo-absorption cross section, it is necessary to calculate matrix elements of d_j. In terms of the creation and annihilation operators $O_\nu^\dagger$ and O_ν we have

$$d_j = \sqrt{\frac{1}{2E_j}}\left(a_j^\dagger + a_j\right) = \sqrt{\frac{1}{2E_j}}\sum_\nu \left[\left(X_j^\nu + Y_j^\nu\right)O_\nu + \left(X_J^{\nu *} + Y_j^{\nu *}\right)O_\nu^\dagger\right], \tag{24}$$

and hence the matrix element $\langle\nu|d_j|0\rangle$ can be written as

$$\langle\nu|d_j|0\rangle = \sqrt{\frac{1}{2E_j}}\left(X_j^{\nu *} + Y_j^{\nu *}\right). \tag{25}$$

In addition, the transition matrix elements must be evaluated in the non-rotating laboratory frame. This is accomplished by first transforming the fixed laboratory coordinates to the frame rotating about the fixed z-axis with rotational frequency ω, and then into the intrinsic frame defined by the Euler angles. To do this, it is necessary to evaluate the matrix elements of the spherical tensors d_μ. Here, we write d_μ in terms of its spherical components, that is

$$d_\mu = \sum_j g_{\mu j} d_j, \tag{26}$$

where the matrix $g_{\mu j}$ is defined by the well known relations

$$d_\mu = \begin{cases} d_3, & \text{if } \mu = 0; \\ \mp\frac{1}{\sqrt{2}}(d_1 \pm d_2), & \text{if } \mu = \pm 1. \end{cases} \tag{27}$$

The matrix elements in the frame rotating about the z-axis become

$$\begin{aligned}\langle\nu|d'_\mu|0\rangle &= \sum_{\mu'}\langle\nu|d_{\mu'}|0\rangle D^{(1)}_{\mu\mu'}(\Omega) \\ &= \sum_{\mu',j} g_{\mu' j}\sqrt{\frac{1}{2E_j}}\left(X_j^{\nu *} + Y_j^{\nu *}\right) D^{(1)}_{\mu\mu'}(\Omega),\end{aligned} \tag{28}$$

where $D^{(1)}_{\mu\mu'}(\Omega)$ is the rotation function for tensors of rank 1.

The GDR cross section to be used in Eqs. (1) is now readily calculable. From Fermi's Golden rule, $\sigma(\alpha,\omega;E)$ evaluated in the intrinsic frame for a nucleus with A nucleons, Z protons, and N neutrons is

$$\sigma_{int}(\alpha,\omega;E) = \frac{4\pi^2 e^2\hbar}{3mc}\frac{2ZN}{A}\sum_{\mu,\nu}|\langle\nu|d_\mu|0\rangle|^2_{\alpha,\omega}E\left[\delta(E-E_\nu(\alpha,\omega)) - \delta(E+E_\nu(\alpha,\omega))\right]. \quad (29)$$

Noting that

$$\delta(E-E') = \frac{1}{2\pi}\int_{-\infty}^{\infty} dt \mathrm{e}^{i(E-E')t} \quad (30)$$

we have

$$\begin{aligned}\sigma_{int}(\alpha,\omega;E) &= \frac{4\pi^2 e^2\hbar}{3mc}\frac{2ZN}{A}\sum_{\mu,\nu}\int_{-\infty}^{\infty} dt|\langle\nu|d_\mu|0\rangle|^2_{\alpha,\omega}E\left[\mathrm{e}^{i(E-E_\nu(\alpha,\omega))t} - \mathrm{e}^{i(E+E_\nu(\alpha,\omega))t}\right],\\ &= \frac{4\pi^2\hbar}{3mc}\frac{2ZN}{A}\sum_{\mu,\nu}\int_{-\infty}^{\infty} dtE\mathrm{e}^{iEt}\\ &\quad \left[\langle 0|d^\dagger_\mu(0)|\nu\rangle_{\alpha,\omega}\langle\nu|d_\mu(t)|0\rangle_{\alpha,\omega} - \langle 0|d^\dagger_\mu(t)|\nu\rangle_{\alpha,\omega}\langle\nu|d_\mu(0)|0\rangle_{\alpha,\omega}\right], \quad (31)\end{aligned}$$

where in the Heisenberg picture $d_\mu(t) = \mathrm{e}^{-iHt}d_\mu(0)\mathrm{e}^{iHt}$. The fact that the experimental giant-dipole resonance has an intrinsic width, Γ_ν, can be accounted for in Eq. (31) by modifying the exponential by $\mathrm{e}^{(iE-\Gamma_\nu/2)t}$ giving

$$\begin{aligned}\sigma_{int}(\alpha,\omega;E) &= \frac{4\pi^2 e^2\hbar}{3mc}\frac{2ZN}{A}\sum_{\mu,\nu}|\langle\nu|d_\mu|0\rangle|^2_{\alpha,\omega}E\\ &\quad [\mathrm{BW}(E,E_\nu(\alpha,\omega),\Gamma_\nu) - \mathrm{BW}(E,-E_\nu(\alpha,\omega),\Gamma_\nu)], \quad (32)\end{aligned}$$

where $\mathrm{BW}(E,E',\Gamma)$ is a Breit-Wigner function

$$\mathrm{BW}(E,E',\Gamma) = \frac{1}{2\pi}\frac{\Gamma}{(E-E')^2+\Gamma^2/4}. \quad (33)$$

In the limit that $\omega = 0$ (i.e. $E_\nu = E_k$), Eq. (32) is a sum of three normalized Lorentzians each with a centroid at $E'_\nu = \sqrt{E_\nu^2 + \Gamma_\nu^2/4}$ and width Γ_ν, and satisfies 100% of the classical sum rule. For finite ω, however, Eq. (32) is a sum of three Lorentzians with a normalization of the order E_ν/E_k, and does not necessarily satisfy 100% of the classical sum rule.

Lastly, in order to evaluate $\sigma(\alpha,\omega;E)$ in the non-rotating laboratory frame, it is necessary to evaluate the matrix elements $\langle\nu|d^{lab}_\mu|0\rangle$ in Eq. (31). These matrix elements may be related to those in the intrinsic frame via Eq. (28) by noting that the transformation from the fixed frame to the rotating frame is accomplished by a rotation about the z-axis by the angle ωt. That is,

$$d_\mu^{lab}(t) = \mathrm{e}^{i\mu\omega t} d'_\mu(t) = \sum_{\mu'} \mathrm{e}^{i\mu\omega t} d_{\mu'}(t) D^{(1)}_{\mu\mu'}(\Omega). \tag{34}$$

From Eq. (31), we see that in addition to mixing the strengths of the various components, the GDR energies are themselves shifted by $-\mu\omega$. Therefore, in the laboratory frame, we have

$$\sigma(\alpha,\omega;E) = \frac{4\pi^2 e^2\hbar}{3mc}\frac{2ZN}{A}\sum_{\nu,\mu}\sum_{\mu,\mu'}\langle 0|d^\dagger_{\mu'}|\nu\rangle_{\alpha,\omega}\langle\nu|d_{\mu''}|0\rangle_{\alpha,\omega} D^{(1)*}_{\mu\mu'} D^{(1)}_{\mu\mu''}$$
$$E[\mathrm{BW}(E, E_\nu(\alpha,\omega)-\mu\omega,\Gamma_\nu) - \mathrm{BW}(E, -(E_\nu(\alpha,\omega)-\mu\omega),\Gamma_\nu)]. \tag{35}$$

IV. SHELL CORRECTIONS

Due to the exponential dependence in Eq. (1), the most important ingredient for the calculation of the GDR strength function is the nuclear free energy. Here, the free energies were computed using the standard Nilsson-Strutinsky [22] procedure extended to finite temperature [23], namely

$$F = F_{LD} + F_N - F_S = F_{LD} + F_{SHL}, \tag{36}$$

where F_{LD} is the liquid-drop free energy evaluated with the parameters of Ref. [24], and F_N and F_S are the Nilsson and Strutinsky components comprising the shell correction, F_{SHL}, to the free energy. In this work, the Nilsson parameters were taken from Ref. [25]. For the most part, the shell corrections for ^{120}Sn were found to be quite small (a few hundred keV at $T \sim$1.25 MeV), and for all practical purposes can be ignored. This is primarily due to the fact that the separate proton and neutron contributions are approximately equal in magnitude, but opposite in sign, and, hence, essentially cancel. This is in sharp contrast to the strong coherence found in ^{208}Pb, where, at low temperatures, strong shell corrections (~ -14 MeV at $T = 0$ MeV) are found that favor the spherical shape.

We have also investigated the influence of the pairing interaction, and have found that effects due to pairing are significant only for temperatures below $\sim$ 0.75 MeV, which is a

lower temperature than for which experiments have been performed. In addition, Nilsson-Strutinsky calculations that include pairing, indicate that, for the most part, the effects on the free energy are negligible. This is because ^{208}Pb is a doubly closed-shell nucleus with pairing gaps equal to zero for the spherical shape, and in ^{120}Sn, as was the case for the free energy without pairing disscussed above, the separate proton and neutron contributions tend to cancel, leading to a free energy whose deformation dependence is essentially that of the liquid drop.

We note that a numerical determination of the effects of thermal fluctuations in Eq. (1) in general requires an exploration of the five dimensional space spanned by the deformation and orientation degrees of freedom, in which a large number of points are required in order to assure sufficient accuracy (especially at finite angular momentum). In this regard, a Nilsson-Strutinsky calculation for each point may be too time consuming. Therefore, it is useful to parameterize the free energy using functions that mimic the behavior of the Nilsson-Strutinsky calculation as closely as possible. It has been pointed out [26] that, being a scalar quantity, the free energy must be a function of the rotational invariants of the quadrupole deformation, that is

$$F(T,\beta,\gamma) = F_0(T) + A(T)\beta^2 - B(T)\beta^3\cos(3\gamma) + C(T)\beta^4 + ... \tag{37}$$

Although this Landau parameterization gives a good overall description of the free energy, in particular regarding to shape transitions, it may not be adequate for the evaluation of Eq. (1) because at somewhat larger deformations Eq. (37) deviates from the Nilsson-Strutinsky calculation, often giving a much stiffer free energy. This is principally because Eq. (37) attempts to combine both the liquid-drop free energy and shell corrections, $F_{SHL} = F_N - F_S$, into the same parameterization. An alternative approach is to parameterize instead only the shell corrections to the free energy using a function of the rotational invariants.

Exhibited in Fig. 2 (solid points) are shell corrections to the free energy at $\omega_{rot} = 0$ as a function of temperature for oblate ($\gamma = \pi/3$), prolate ($\gamma = 0$), and triaxial ($\gamma = \pi/6$) deformations for ^{208}Pb. The general overall behavior of F_{SHL} is to decrease with

temperature, gradually melting ($F_{SHL} \approx 0$ MeV) for temperatures of the order $T = 2.5$ MeV, and that they tend to oscillate with deformation, but appearing to be damped at larger β. In this light, it is possible to parameterize F_{SHL} with a series of functions that are in fact themselves functions of the rotational invariants β^2, $\beta^3 \cos(3\gamma)$, etc... One possible parameterization is

$$F_{SHL}(\beta, \gamma, T) = \sum_{l=0}^{even} A_l j_l(B_l \beta) C_l T / \sinh(C_l T) + \sum_{l=3}^{odd} A_l j_l(B_l \beta) \cos(3\gamma) C_l T / \sinh(C_l T), \tag{38}$$

where the j_l are spherical Bessel functions. We note that $C_l T / \sinh(C_l T)$ is the expected attenuation behavior as a function temperature when the single-particle Hamiltonian is a degenerate harmonic oscillator [19].

The parameters A_l, B_l, and C_l can be determined in the following manner. First, carry out a Nilsson-Strutinsky calculation for oblate, prolate and triaxial shapes up to $\beta = 1.0$, and for temperatures between $T = 0.25$ and 3.0 Mev. Then fit both parameters A_l and B_l to the Nilsson-Strutinsky calculation at $T = 0.25$ MeV for all three shapes simultaneously. Note that at $\beta = 0$, the free energy is completely determined by A_0, and as such is not fit upon. In addition, note that the $\gamma = \pi/6$ points are dependent only on the even functions in Eq. (38). Typically, the number of terms in Eq. (38) can be truncated to $l \sim 5$. With the parameters B_l determined at $T = 0.25$ MeV, these same values are then used to fit the A_l values at all other temperatures, giving the sequence $\{A_l(T_i)\}$, which is then fit to the function $A_l C_l T / \sinh(C_l T)$. Shown in Fig. 2 with the solid line are the results of the parameterization of the shell corrections to the free energy for ^{208}Pb, and the associated parameters are listed in Table I. Generally speaking, the parameterization of Eq. (38) gives a good overall reproduction of the shell corrections, F_{SHL}, that is rather quick to implement with Eq. (1).

We note one feature of the parameterization for ^{208}Pb is that the parameterized shell corrections tend to "melt" a little too quickly. For example, for $T > 1.5$ MeV the parameterized shell corrections underestimate the Nilsson-Strutinsky values by a few hundred keV.

It is to be noted, however, that at these temperatures, this amounts to a relatively small change in the overall deformation dependence of the total free energy, which, in addition to be divided by the temperature in the Boltzman factor, $\mathrm{e}^{-F/T}$ is at basically dominated by the liquid-drop component.

In addition to the free energy, shell structure can also modify the moments of inertia. Again, we employ the Nilsson-Strutinsky procedure at finite rotational frequency, and obtain shell corrections to the rigid-body moments of inertia, namely

$$I = I_{rigid} + I_N - I_S = I_{rigid} + I_{SHL}, \tag{39}$$

where here the rigid-body values were evaluated with the radius $R = 1.2A^{1/3}$. Choosing the rotational frequency along the z-axis, the leading behavior as a function of rotational frequency for each of the free energy components in Eq. (36) is given by

$$F(\beta, \gamma, T, \omega) = F(\beta, \gamma, T, \omega = 0) - \tfrac{1}{2} I_3(\beta, \gamma, T)\omega^2. \tag{40}$$

The moments of inertia I_3 can then be obtained by performing a quadratic fit to the free energy components.

In a manner similar to the shell corrections to the free energies, the shell corrections to the moments of inertia may also be parameterized by series of Bessel functions, i.e.,

$$\begin{aligned} I_3^{SHL}(\beta, \gamma, T) = & \sum_{l=0}^{even} A_l^I j_l(B_l^I \beta) C_l^I T / \sinh(C_l^I T) \\ & + \sum_{l=3}^{odd} A_l^I j_l(B_l^I \beta) \cos(3\gamma) C_l^I T / \sinh(C_l^I T) \\ & + \sum_{l \geq 1} \alpha_l j_l(\kappa_l \beta) \cos(\gamma + 2\pi/3) \eta_l T / \sinh(\eta_l T), \end{aligned} \tag{41}$$

where the third term in the sum is included because of rotational invariance arguments for the moment of inertia [6]. Once the third component of the moment of inertia is determined as a function of T, β, γ, the remaining two components are obtained by the relations [6]

$$\begin{aligned} I_1(T, \beta, \gamma) &= I_3(T, \beta, \gamma + 2\pi/3), \\ I_2(T, \beta, \gamma) &= I_3(T, \beta, \gamma - 2\pi/3). \end{aligned} \tag{42}$$

The parameters A_l^I, B_l^I, C_l^I, α_l, κ_l and η_l were determined in a similar manner as those for the free energy in Eq. (38). Again, the shell corrections for ^{120}Sn were found to be small and negligible. For comparison, both the parameterized and Nilsson-Strutinsky shell corrections to the moment of inertia for ^{208}Pb are shown in Fig. 3 as a function of temperature and for the deformations $\gamma = \pi/3,\ \pi/6,\ 0,\ -\pi/3,$ and $-2\pi/3$. The most important feature is the strong shell corrections at $\beta = 0$ that significantly reduced the moment inertia below the rigid-body value.

Of particular importantance for the moments of inertia is the fact that the spin-orbit and l^2 terms in the Nilsson Hamiltonian lead to moments of inertia that are approximately 20-30% larger than the corresponding rigid-body values [27]. As such, the shell corrections to the moments of inertia used here were reduced by 25%, which corresponds to the average difference between the rigid-body and Strutinsky moments of inertia. The corresponding parameters A_l^I, B_l^I, C_l^I, α_l, κ_l and η_l are then listed in Table II for ^{208}Pb.

Because of the $\mathcal{I}^{-3/2}$ dependence in the "effective" volume element in Eq. (1), it might be expected that the strong shell corrections to the moment of inertia in ^{208}Pb would significantly affect the GDR strength function, as they appear to give a stronger preference to the spherical shape. We find, however, that because of the β^4 factor in $\mathcal{D}[\alpha]$, the strong shell corrections in $\mathcal{I}$ favoring the spherical shape have very little effect on the FWHM of the GDR at low spin beyond that produced by the free energy. This is exhibited in Fig. 4, where an "effective" weight factor (which for the sake of simplicity ignores the $\sin 3\gamma$ factor) $W = \beta^4/\mathcal{I}^{3/2}\mathrm{e}^{-F/T}$ is plotted for oblate and prolate shapes at $T = 1.0$ MeV for various combinations of the shell corrections. In the top panel of the figure, the weight factor is plotted including shell corrections to the free energy as well as with and without shell corrections to the moments of inertia, whereas the corresponding figure without shell corrections to the free energy is shown in the bottom part of the figure. In both cases, it is seen that the overall behavior of the weight function is governed by the exponential of the free energy, which is plotted in the upper right-hand panel. In addition, the ratio $\mathcal{I}_{LD}/\mathcal{I}_{SHL}$ is shown in the lower left-hand panel, where it is seen that without the β^4 factor the spherical shape would

have approximately 40% more weight when shell corrections to the moments of inertia are included.

V. RESULTS

In this section we present the results of a systematic comparison between theoretical calculations and recent experimental data [13] as a function of temperature for both ^{120}Sn and ^{208}Pb. The thermally averaged GDR cross sections were computed using Eqs.(1) and (35). In keeping with experimental findings [21], the intrinsic dipole widths, Γ_ν were taken to be dependent on the centroid energy E_ν via $\Gamma_\nu = \Gamma_0(E_\nu/E_0)^\delta$, where E_0 and Γ_0 are the centroid and width for spherical shape and $\delta \approx 1.8$. The parameters E_0 and Γ_0 were taken from ground-state data and are $E_0 = 14.99$ MeV and $\Gamma_0 = 5.0$ MeV for ^{120}Sn and $E_0 = 13.65$ MeV and $\Gamma_0 = 4.0$ MeV for ^{208}Pb, respectively. Finally, in accordance with the considerable theoretical evidence presented in Ref. [2], the intrinsic width Γ_0 is taken to be independent of temperature throughout this work.

Shown in Fig. 5 are the results obtained for the FWHM of the GDR strength function for both ^{120}Sn and ^{208}Pb as a function of temperature in comparison with recent experimental data. The solid line represents the theoretical values obtained with zero angular momentum. The dependence of the FWHM for ^{120}Sn and ^{208}Pb on angular momentum at $T = 1.6$ MeV is illustrated in Fig. 6, where it is seen that for $J \leq 25\hbar$ the FWHM is essentially unchanged from the $J = 0\hbar$ value. Given that the largest average angular momentum in the systems studied experimentally is of the order $20\hbar$ [13], the effects due to angular momentum on the data set of interest are then expected to be negligible.

As is seen from Fig. 5, theory provides an overall account of the experimental findings. The dependence of the FWHM on temperature is quite different between ^{120}Sn and ^{208}Pb. The FWHM in ^{208}Pb appears to be suppressed at lower temperatures relative to ^{120}Sn. This is due to the rather strong shell corrections in ^{208}Pb that favor the spherical shape at low temperatures. The affect of such strong shell corrections is to limit the influence

of thermal fluctuations at low temperatures, thereby reducing the observed width. This is also illustrated in Fig. 5, where the dotted line in the panel for ^{208}Pb indicates the FWHM assuming no shell corrections. We note that the shell correction effect and the angular momentum dependence was also observed for ^{140}Ce in Ref. [5]. The fact that the adiabatic model slightly overestimates the FWHM maybe due to: (1) uncertainties in the extracted temperature; (2) the shell corrections being more persistent at higher temperatures than predicted by Nilsson-Strutinsky calculations; (3) the fact that the experimental strength functions were fit to a single Lorentzian, while theoretically they are obtained from the superposition of many Lorentzians; and/or (4) the presence of non-adiabatic effects that would lead to a motional narrowing of the FWHM [7]. In keeping with point (1) above, one can mention that the temperatures inferred from experiment are sensitive to the choice of the level-density parameter, and, as a consequence, are uncertain at the level of approximately 0.2 MeV.

The FWHM shown in Fig. 5 are essentially consistent with the adiabatic picture for the GDR in hot nuclei, and do not present any evidence for the phenomenon known as motional narrowing [7,8], which tends to lessen the effects of thermal broadening on the resonance, and, hence, reduce the FWHM. As is pointed out in Ref. [8], however, because of a lack of reliable theoretical estimates for the time scales associated with thermal fluctuations, the FWHM is not sufficient in of itself to exclude motional narrowing. This is particularly true when the time scales for β and γ degrees of freedom are much faster than those associated with the orientation of the system. In this case, both the response function and the angular distribution a_2 coefficient are needed in order to make a differentiation between the two regimes.

We note some slight discrepancies between the adiabatic model and experiment for ^{120}Sn. To begin with, the FWHM at $T = 1.24$ MeV is significantly lower than the theoretical prediction and is difficult to explain within the framework of the model. This datum seems to point to the existence of strong shell corrections that quickly disappear at $T = 1.5$ MeV, which is in disagreement with the expectations of the Nilsson-Strutinsky procedure. At

higher temperatures, $T \approx 2.8 - 3.1$ MeV, the experimental FWHM is somewhat larger than the theoretical values, and may indicate a systematic trend to be observed at still higher temperatures. Shown in Fig. 7 is the FWHM for ^{120}Sn at $T = 3.12$ MeV as a function of the intrinsic width Γ_0. At this temperature, the experimental FWHM is 11.5 ± 1.0 MeV, and we may infer from this datum a value of $\Gamma_0 = 7.7^{+1.8}_{-2.1}$ MeV, as indicated by the solid square (11.5 MeV) and open circles (± 1 MeV) in Fig. 7. We note, however, that this is consistent with the concept that the width observed for the GDR in hot nuclei should be increased because of the evaporation of particles from the compound nucleus [11]. At higher excitation energies, the decay rate for particle evaporation increases, and, because of the uncertainty principle, the energy of an emitted GDR photon cannot be known with a precision better than $\Gamma_{cn} = \Gamma_{ev}^{before} + \Gamma_{ev}^{after}$, where $\Gamma_{ev}^{before(after)}$ is the width for particle evaporation *before* and *after* the emission of the GDR photon. To account for this effect in our calculations, we note that the FWHM shown in Fig. 5 are obtained from the full response function, which also includes splittings due to the superposition of the various intrinsic modes. On the other hand, Γ_{cn} represents an uncertainty in the GDR photon energy due to the lifetime of the initial and final states. As such, Γ_{cn} should be folded into the GDR response function by increasing the intrinsic widths via $\Gamma'_\nu \to \Gamma_\nu + \Gamma_{cn}$. In order to estimate Γ_{cn} for ^{120}Sn we refer to Fig. 2 of ref. [10], where Γ_{ev} is plotted as a function of excitation energy for various values of the level-density parameter a (which is conventionally defined as $a = A/\kappa$ MeV^{-1}, and values of Γ_{ev} are plotted for $\kappa = 8$, 10, and 12). We note that at a given excitation energy, Γ_{ev} exhibits a strong dependence on a. Indeed, at $E_x = 150$ MeV, there is a nearly a factor of three difference between the results for $\kappa = 8$ and 12. This rather strong dependence on a is considerably diminished, however, when converting to temperature, defined as $E_x - E_{GDR} = aT^2$, as is shown in Table III where $\Gamma_{ev}^{before(after)}$ and Γ_{cn} are given as a function of temperature for $\kappa = 10$ and 12. Only at the highest temperatures (≈ 3.5 MeV), where κ is expected to be of the order 12-13, is the difference much greater than a few hundred keV. Taking $\kappa = 12$, we deduce at $T \approx 3.1$ MeV $\Gamma_{cn} \approx 2.1$ MeV, which is in good agreement with the experimental results as is illustrated in

Fig. 7. To further see the influence of the evaporation width, we have computed the FWHM for ^{120}Sn a function of temperature including Γ_{cn} (evaluated with $\kappa = 12$), which is shown in Fig. 5 by the dashed line. On the whole, the inclusion of Γ_{cn} leads to a better overall agreement with experiment.

It is to be noted that although the experimental data for ^{208}Pb do not, as yet, extend to $T \sim 3.0$ MeV, the effects of the particle evaporation width will also be present in ^{208}Pb. We have computed Γ_{ev} for ^{208}Pb using the same method as in Ref. [10] and is displayed in Fig. 8 as a function of excitation energy for $\kappa = 8$, 10, and 12. Also shown in Table IV are values of $\Gamma_{ev}^{before(after)}$ and Γ_{cn} as a function of temperature for $\kappa = 10$ and 12. The FWHM for ^{208}Pb including Γ_{cn} (with $\kappa = 12$) is shown in Fig. 5 with the dashed line, where it is seen that at $T = 3.25$ MeV the FWHM is approximately 2.5 MeV larger than predicted by the adiabatic model. As such, experiments carried out in this temperature range would be a further confirmation of this effect. Finally, as is pointed out in Ref. [10], the particle evaporation width also leads to a maximum excitation energy (or limiting temperature) above which the GDR is not observable. This occurs when $\Gamma_{ev} \sim \Gamma_0$, which for ^{208}Pb corresponds to $E_x \approx 300 - 350$ MeV (or $T \approx 4.2 - 4.5$ MeV).

VI. CONCLUSIONS

We conclude that a systematic study of the FWHM of the GDR as a function of temperature for the nuclei ^{120}Sn and ^{208}Pb confirms, for the first time, the overall theoretical picture of the GDR in hot nuclei at low spin. In particular, the role played by adiabatic, large-amplitude thermal fluctuations of the nuclear shape. In fact, overall agreement between theory and experiment is observed over a range of temperatures for both ^{120}Sn and ^{208}Pb, which display quite different behaviors for the FWHM as a function of temperature. This difference can be attributed to the presence of strong shell corrections favoring spherical shapes in ^{208}Pb that are absent in ^{120}Sn. Finally, the increase in the FWHM over that expected from thermal averaging at temperatures of the order 3.0 MeV is in accordance

with the increase expected from the particle evaporation of the compound system.

ACKNOWLEDGEMENTS

Oak Ridge National Laboratory is managed for the U.S. Department of Energy by Lockheed Martin Energy Research Corp. under contract No. DE–AC05–96OR22464.

REFERENCES

[1] K.A. Snover, Annu. Rev. Nucl. part. Sci. **36**, 545 (1986); J.J. Gaardhøje, Annu. Rev. Nucl. Part. Sci. **42**, 483 (1992).

[2] P.F. Bortignon *et al.*, Nucl. Phys. **A460**, 149 (1986); F.V. De Blasio, *et al.* Phys. Rev. Lett. **68**, 1663 (1992); P. Donati, N. Giovanardi, P.F. Bortignon, and R.A. Broglia, Phys. Lett. **B** (in press).

[3] V. Baran, M. Colonna, M. Di Toro, A. Guarnera, V.N. Kondratyev, and A. Smerzi, Nucl. Phys. **A599**, 29c (1996).

[4] M. Gallardo *et al.*, Nucl. Phys. **A443**, 415 (1985); J.M. Pacheco, C. Yannouleas, and R.A. Broglia, Phys. Rev. Lett. **61**, 294 (1988).

[5] Y. Alhassid, B. Bush, and S. Levit, Phys. Rev. Lett. **61**, 1926 (1988).

[6] Y. Alhassid and B. Bush, Nucl. Phys. **A509**, 461 (1990).

[7] B. Lauritzen *et al.*, Phys. Lett. **B207**, 238 (1988); Y. Alhassid and B. Bush, Phys. Rev. Lett. **63**, 2452 (1989); W.E. Ormand *et al.*, Phys. Rev. Lett. **64**, 2254 (1990).

[8] W.E. Ormand *et al.*, Phys. Rev. Lett. **69**, 2905 (1992).

[9] J.J. Gaardhøje *et al.*, Phys. Rev. Lett. **59**, 1409 (1987); A. Bracco *et al.*, Nucl. Phys. **A519**, 47c (1990); K. Yoshida *et al.*, Phys. lett. **B245**, 7 (1990); J. Kasagi *et al.*, Nucl. Phys. **A538**, 585c (1992); J. Kasagi *et al.*, Nucl. Phys. **A557**, 221c (1993); J.H. Le Faou *et al.*, Phys. Rev. Lett. **72**, 3321 (1994).

[10] P.F. Bortignon, A. Bracco, D. Brink, and R.A. Broglia, Phys. Rev. Lett. **67**, 3360 (1991).

[11] Ph. Chomaz, Phys. Lett. **B347**, 1 (1995).

[12] A. Bracco *et al.*, Phys. Rev. Lett. **74**, 3748 (1995); A. Bracco *et al.*, *Proc. of the*

Groningen Conference on Giant Resonances, 28 June - 1 July, 1995, Nucl. Phys. **A599**, 83c (1996).

[13] E. Ramakrishnan *et al.*, *Proc. of the Groningen Conference on Giant Resonances, 28 June - 1 July, 1995*, Nucl. Phys. **A599**, 49c (1996); E. Ramakrishnan *et al.*, Phys. Rev. Lett. **76**, 2025 (1996).

[14] W.E. Ormand, P.F. Bortignon, and R.A. Broglia, Phys. Rev. Lett. (in press).

[15] Y. Alhassid and N. Whelan, Nucl. Phys. **A565**, 427 (1993).

[16] W.E. Ormand, P.F. Bortignon, R.A. Broglia, to be published.

[17] J.L. Egido, and P. Ring, Phys. Rev. **C25**, 3239 (1982); M.E. Faber, J.L. Egido, and P. Ring, Phys. Lett. **127B**, 5 (1983); P. Ring, L.M. Robledo, J.L. Egido, and M. Faber, Nucl. Phys. **A419**, 261 (1984); W. Besold, P.-G. Reinhard, and C. Toepffer, Nucl. Phys. **A431**, 1 (1984); H. Sagawa and G.F. Bertsch, Phys. Lett. **B146**, 138 (1984); M. Gallardo, M. Diebel, T. Døssing, and R.A. Broglia, Nucl. Phys. **A443**, 415 (1985).

[18] K. Neergård, Phys. Lett. **110B**, 7 (1982).

[19] A. Bohr and B.R. Mottelson, *Nuclear Structure* (Benjamin, Reading, MA, 1975), Vol. II.

[20] D.L. Hill and J.A. Wheeler, Phys. rev.**89**, 1102 (1953)

[21] P. Carlos *et al.*, Nucl. Phys. **A219**, 61 (1974).

[22] V.M. Strutinsky, Yad. Fiz. **3**, 614 (1966) [Sov. J. Nucl. Phys. **3**, 449 (1966)]; Ark. Fys. **36**, 629 (1966); Nucl. Phys. **A95**, 420 (1967); Nucl. Phys. **A122**, 1 (1968).

[23] M. Brack and P. Quentin, Nucl. Phys. **A361**, 35 (1981).

[24] C. Guet *et al.*, Phys. Lett. **B205**, 427 (1988).

[25] S.G. Nilsson *et al.*, Nucl. Phys. **A131**, 1 (1969).

[26] S. Levit ad Y. Alhassid, Nucl. Phys. **A413**, 439 (1984).

[27] K. Neergård, H. Toki, M. Ploszczack, and A. Faessler, Nucl. Phys. **A287**, 48 (1977).

TABLES

TABLE I. Parameters in Eq. (38) to define the shell corrections to the free energy in ^{208}Pb.

l	A_l	B_l	C_l
0	-13.706	13.764	3.011
2	-6.448	10.357	3.122
3	6.68	8.159	2.408
5	19.50	23.882	3.146

TABLE II. Parameters in Eq. (41) to define the shell corrections to the moment of inertia in ^{208}Pb.

l	A_l	B_l	C_l
0	-87.653	13.764	3.108
2	-49.343	10.357	3.026
3	28.532	8.159	3.068
5	80.810	23.791	3.558
l	α_l	κ_l	η_l
1	-22.910	8.334	2.979

TABLE III. Values of $\Gamma_{cn} = \Gamma_{ev}^{before} + \Gamma_{ev}^{after}$ for ^{120}Sn obtained from Fig. 2 of Ref. [10] as a function of temperature and the level-density parameter defined as $a = A/\kappa$ MeV^{-1}. All quantities are given in MeV

T		$\kappa = 10$				$\kappa = 12$		
	E_x	Γ_{ev}^{before}	Γ_{ev}^{after}	Γ_{cn}	E_x	Γ_{ev}^{before}	Γ_{ev}^{after}	Γ_{cn}
1.25	34	0.03	0.00	0.03	31	0.06	0.02	0.08
1.50	42	0.06	0.03	0.09	38	0.10	0.05	0.15
1.75	52	0.09	0.06	0.17	46	0.13	0.06	0.19
2.00	63	0.14	0.08	0.22	55	0.20	0.11	0.31
2.25	76	0.22	0.12	0.34	66	0.33	0.17	0.50
2.50	90	0.37	0.21	0.58	78	0.52	0.29	0.81
2.75	106	0.61	0.38	0.99	91	0.71	0.49	1.20
3.00	123	0.83	0.63	1.46	105	0.95	0.70	1.65
3.25	142	1.12	0.89	2.01	121	1.31	0.97	2.28
3.50	162	1.45	1.19	2.64	138	1.72	1.36	3.08

TABLE IV. Values of $\Gamma_{cn} = \Gamma_{ev}^{before} + \Gamma_{ev}^{after}$ for ^{208}Pb as a function of temperature and the level-density parameter defined as $a = A/\kappa$ MeV^{-1}. All qunatities are given in MeV.

T		$\kappa = 10$				$\kappa = 12$		
	E_x	Γ_{ev}^{before}	Γ_{ev}^{after}	Γ_{cn}	E_x	Γ_{ev}^{before}	Γ_{ev}^{after}	Γ_{cn}
1.50	61	0.05	0.02	0.07	53	0.07	0.02	0.09
1.75	77	0.10	0.04	0.14	67	0.11	0.06	0.17
2.00	97	0.24	0.12	0.36	83	0.23	0.13	0.36
2.25	119	0.39	0.27	0.66	102	0.46	0.27	0.73
2.50	144	0.64	0.47	1.13	122	0.65	0.50	1.15
2.75	171	0.90	0.76	1.66	145	1.01	0.77	1.78
3.00	201	1.33	1.10	2.43	170	1.38	1.15	2.53
3.25	234	1.73	1.52	3.25	197	1.90	1.58	3.48
3.50	269	2.20	2.01	4.21	226	2.42	2.12	4.54

FIGURES

FIG. 1. The free energy for ^{106}Sn is plotted (lower panel) along the oblate noncollective ($\beta < 0$) and prolate collective ($\beta > 0$) axes at a temperature of 2 MeV and a rotational frequency of 1.25 MeV ($\langle J \rangle \approx 55\hbar$). In the upper panel, the Boltzman weight factor $\exp[-(F - F_{eq})/T]$, where F_{eq} is the minimum of the free energy below the saddle point, is plotted.

FIG. 2. Nilsson-Strutinsky shell corrections (solid squares) to the free energy for ^{208}Pb as a function of temperature for oblate ($\gamma = \pi/3$), triaxial ($\gamma = \pi/6$), and prolate ($\gamma = 0$) shapes at zero angular momentum. The parameterization to the shell corrections given by Eq. (38) is represented by the solid line.

FIG. 3. Nilsson-Strutinsky shell corrections (solid squares) to the moments of inertia for ^{208}Pb for $\gamma = \pi/3$, $\pi/6$, 0, $-2\pi/3$, and $-\pi/3$. The parameterization to the shell corrections given by Eq. (41) is represented by the solid line. The temperature for each panel is the same as in Fig. 2.

FIG. 4. The weight function $W(\beta) = \beta^4/\mathcal{I}^{3/2}\mathrm{e}^{-F/T}$ at $T = 1.0$ MeV for prolate ($\beta > 0$) and oblate ($\beta < 0$) shapes. In panel (a), $W(\beta)$ includes shell corrections to the free energy, F_{SHL}, as well as with (dotted line) and without (solid line) shell corrections to the moments of inertia. In panel (b), the same quantities are plotted without shell corrections to the free energy, i.e., $F = F_{LD}$. The free energy with and without shell corrections is plotted in panel (c), and the factor $(\mathcal{I}_{LD}/\mathcal{I}_{SHL})^{3/2}$ is plotted in panel (d).

FIG. 5. The FWHM of the GDR strength function as a function of temperature for ^{120}Sn and ^{208}Pb. Experimental data are represented by the filled circles, while the solid line represents the theoretical results obtained for $J = 0\hbar$. For ^{208}Pb, the dotted line is the FWHM obtained assuming no shell corrections. For ^{120}Sn and ^{208}Pb, the dashed line represents the FWHM obtained by including the increase to the intrinsic width, Γ_{cn}, due to the evaporation of particles from the compound system.

FIG. 6. The FWHM in ^{120}Sn (dashed line) and ^{208}Pb (solid line) at $T = 1.6$ MeV as a function of angular momentum.

FIG. 7. The FWHM in ^{120}Sn at $T = 3.12$ MeV as a function of the intrinsic width Γ_0 (solid line). The experimental value of 11.5 ± 1.0 MeV is represented by the filled square (11.5 MeV) and the open circles (± 1 MeV).

FIG. 8. The particle evaporation width, Γ_{ev}, for ^{208}Pb as a function of excitation energy for three values of the level-density parameter, i.e. $\kappa = 8$, 10, and 12 (note $a = A/\kappa$ MeV^{-1}).

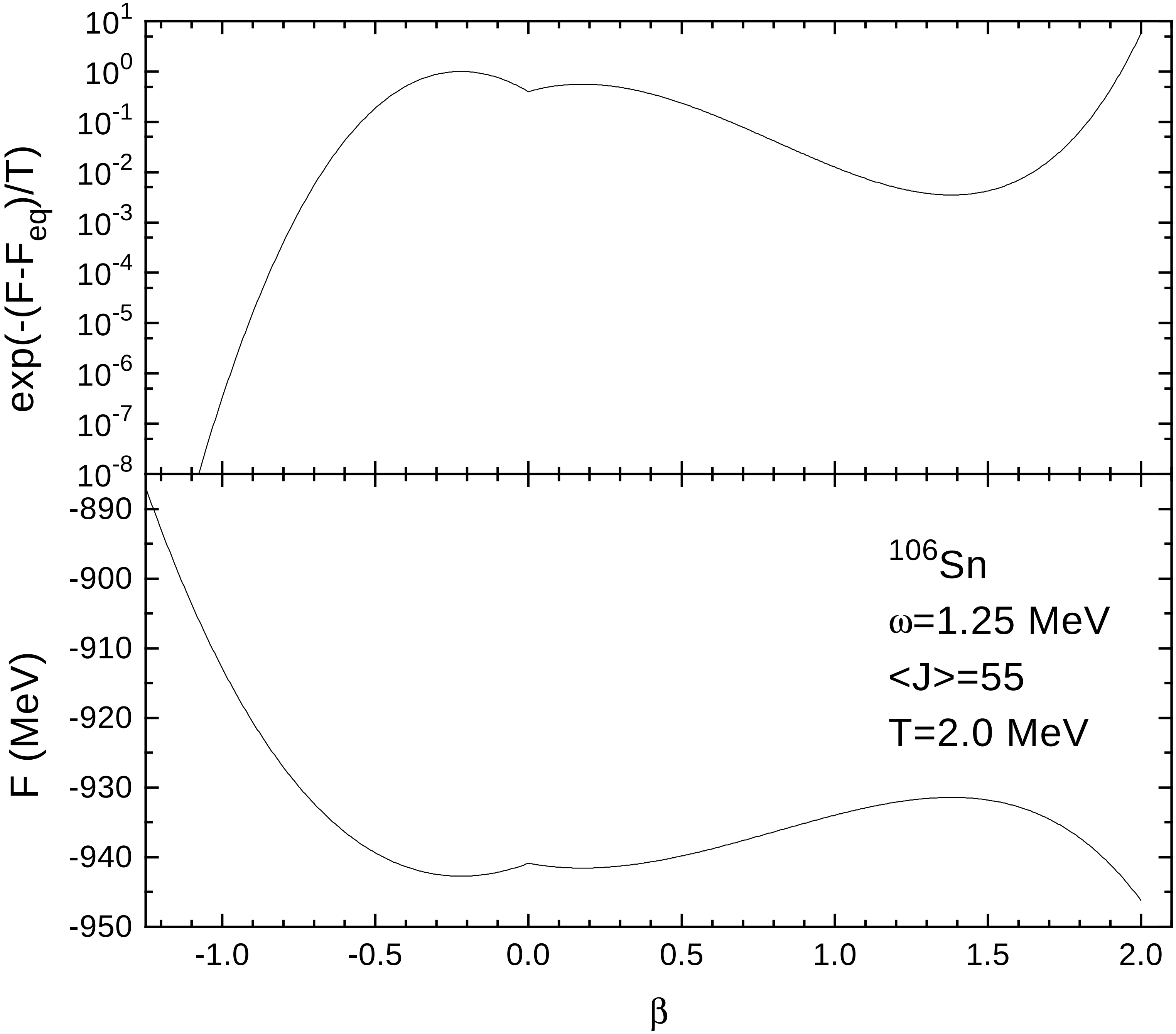

10^{1}
10^{0}
10^{-1}
10^{-2}
10^{-3}
10^{-4}
10^{-5}
10^{-6}
10^{-7}
10^{-8}
$\exp(-(F-F_{eq})/T)$
-890
-900
-910
-920
-930
-940
-950
F (MeV)
^{106}Sn
ω=1.25 MeV
<J>=55
T=2.0 MeV
-1.0
-0.5
0.0
0.5
1.0
1.5
2.0
β

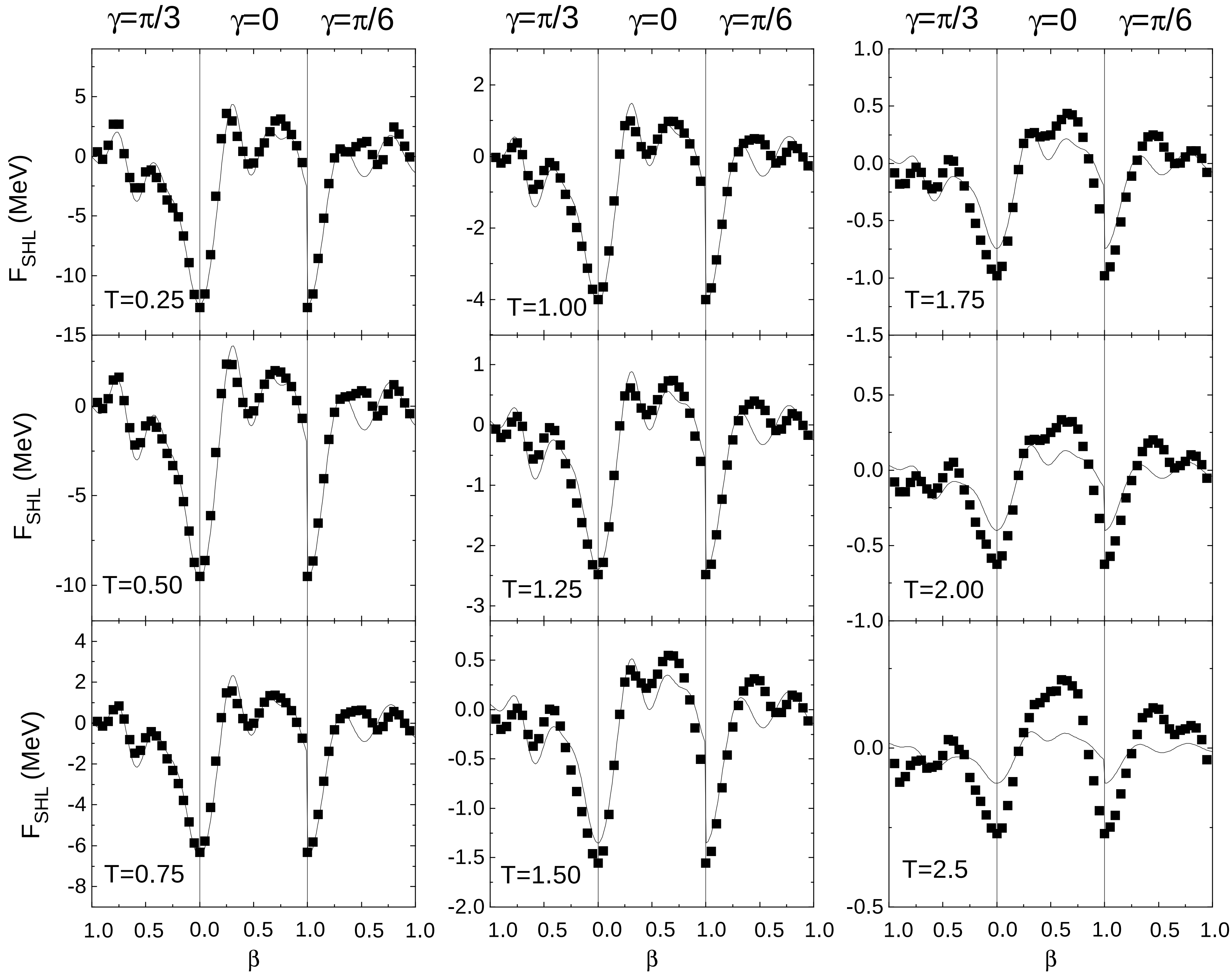

γ=π/3
γ=0
γ=π/6
F_SHL (MeV)
T=0.25
T=0.50
T=0.75
T=1.00
T=1.25
T=1.50
T=1.75
T=2.00
T=2.5
β

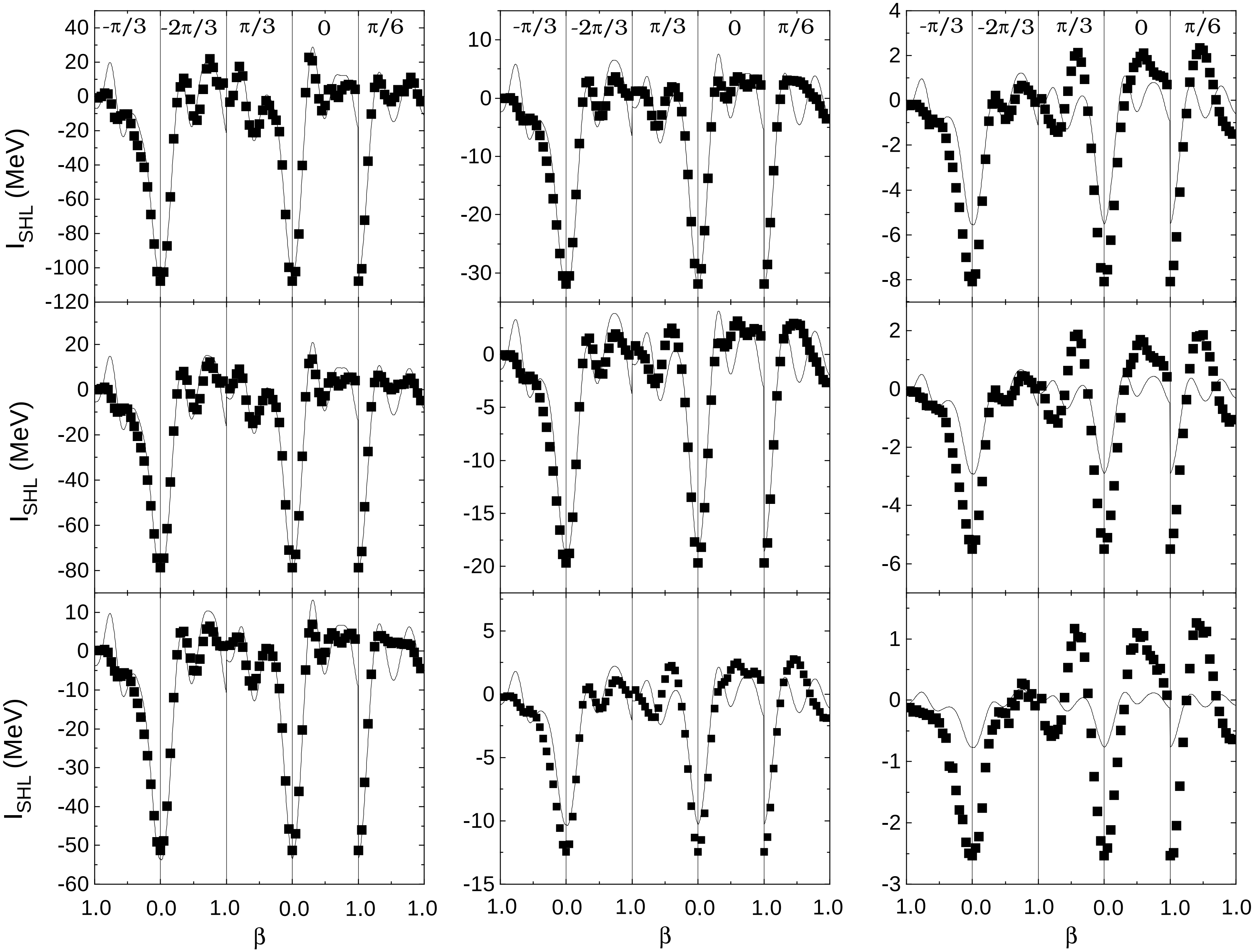

-π/3
-2π/3
π/3
0
π/6
I_{SHL} (MeV)
β
1.0
0.0

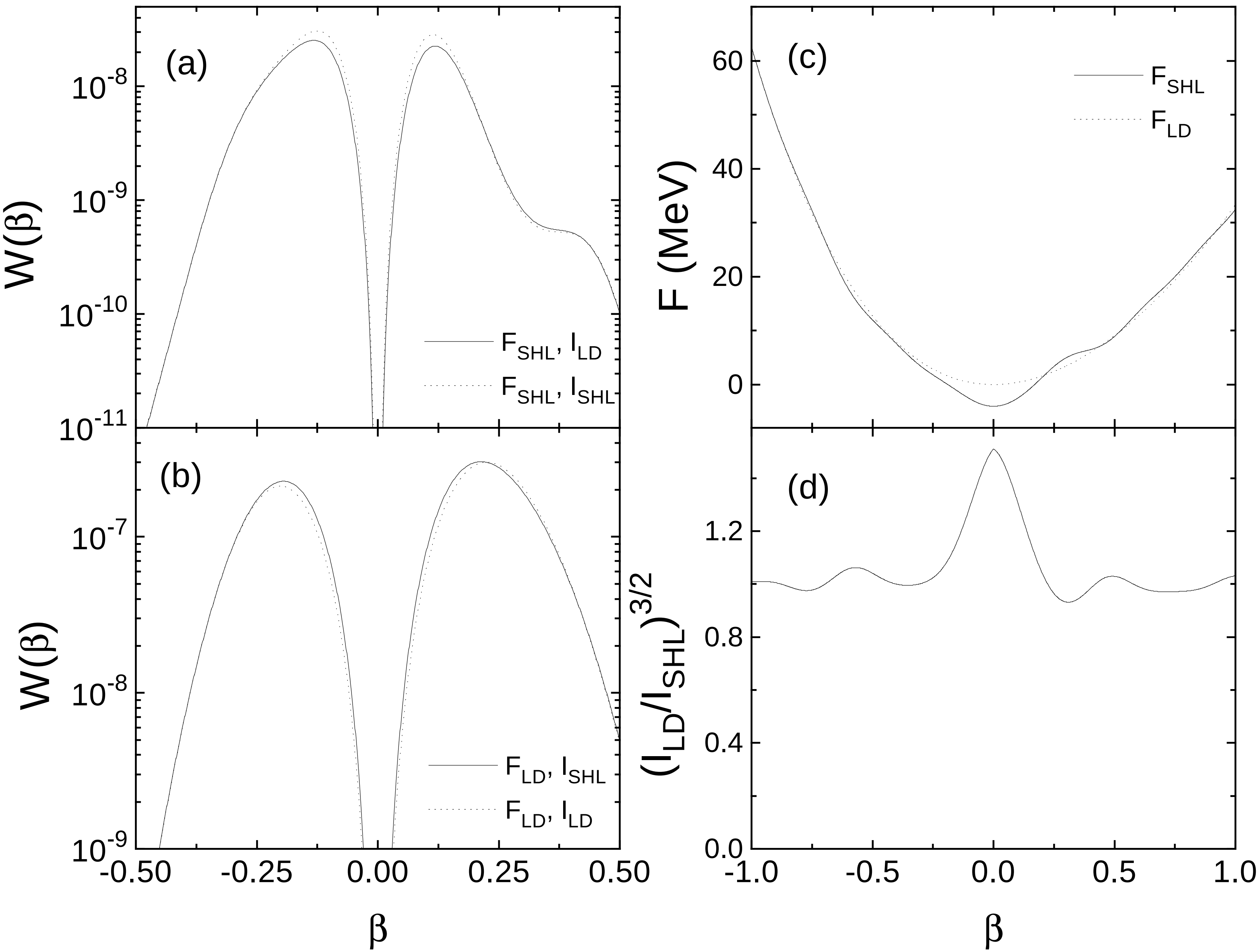

(a)
(b)
(c)
(d)
W(β)
W(β)
F (MeV)
$(I_{LD}/I_{SHL})^{3/2}$
β
β
F_{SHL}, I_{LD}
F_{SHL}, I_{SHL}
F_{LD}, I_{SHL}
F_{LD}, I_{LD}
F_{SHL}
F_{LD}

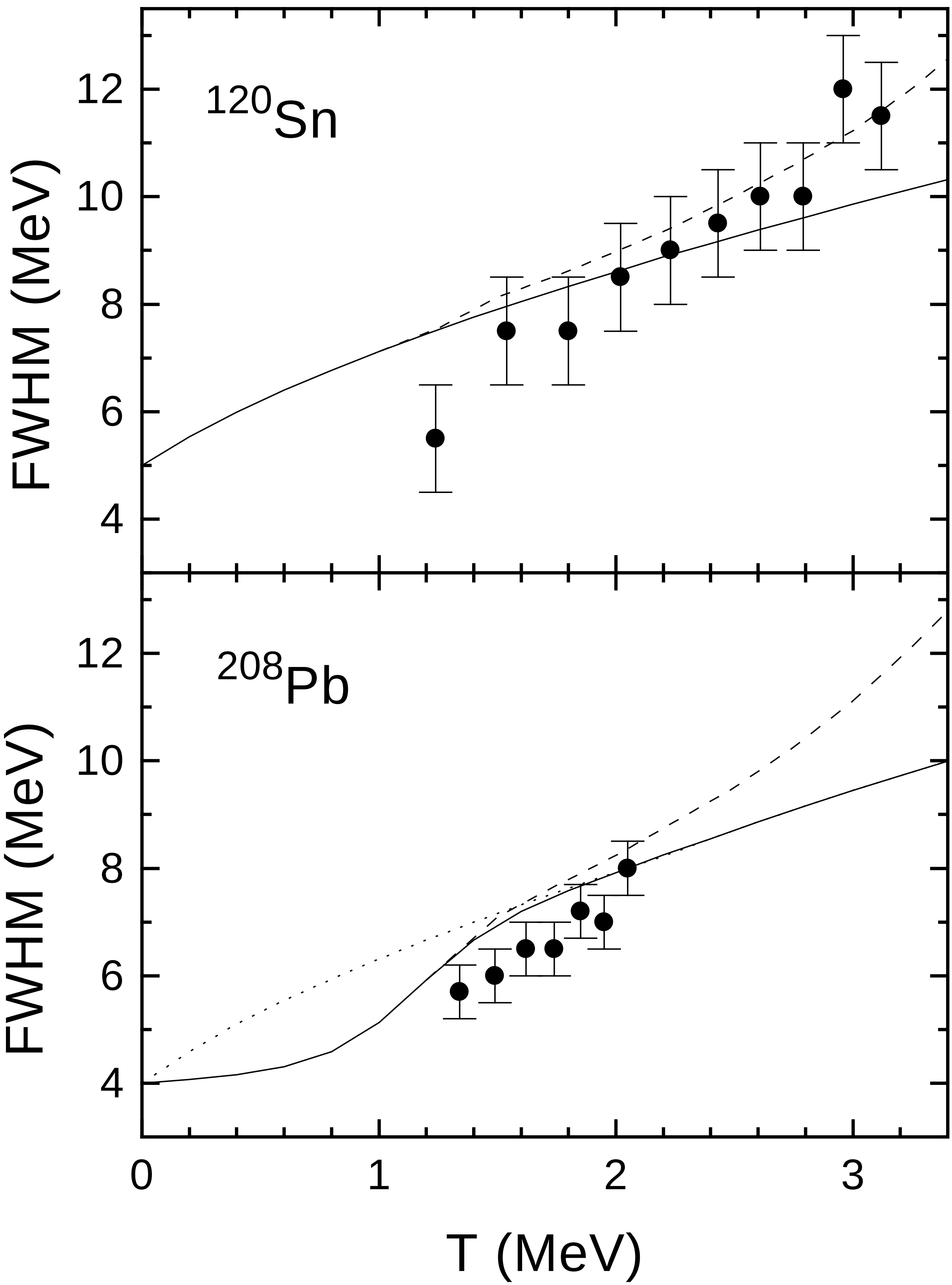

120Sn
208Pb
FWHM (MeV)
FWHM (MeV)
4
6
8
10
12
0
1
2
3
T (MeV)

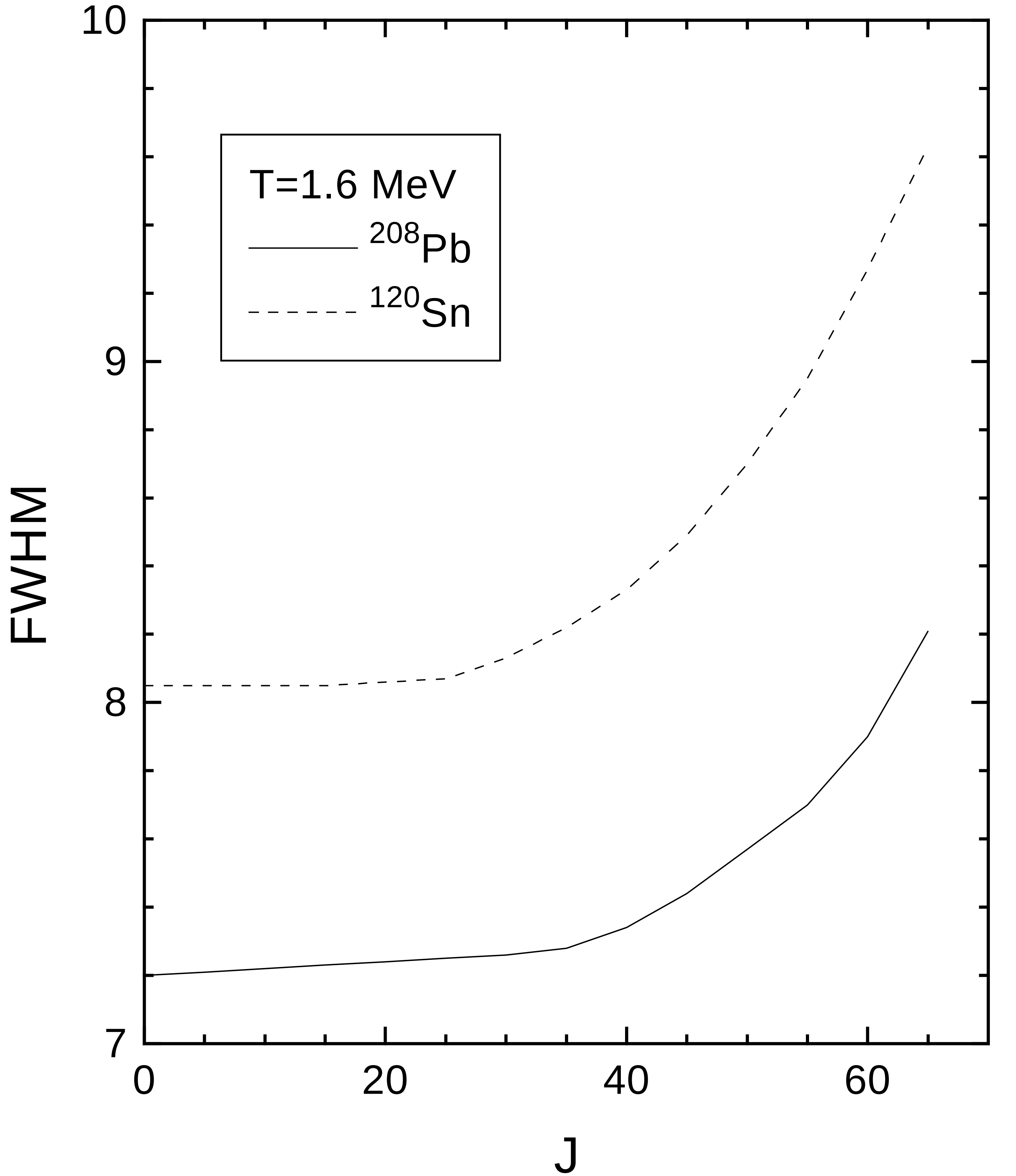

T=1.6 MeV
^{208}Pb
^{120}Sn
FWHM
J
10
9
8
7
0
20
40
60

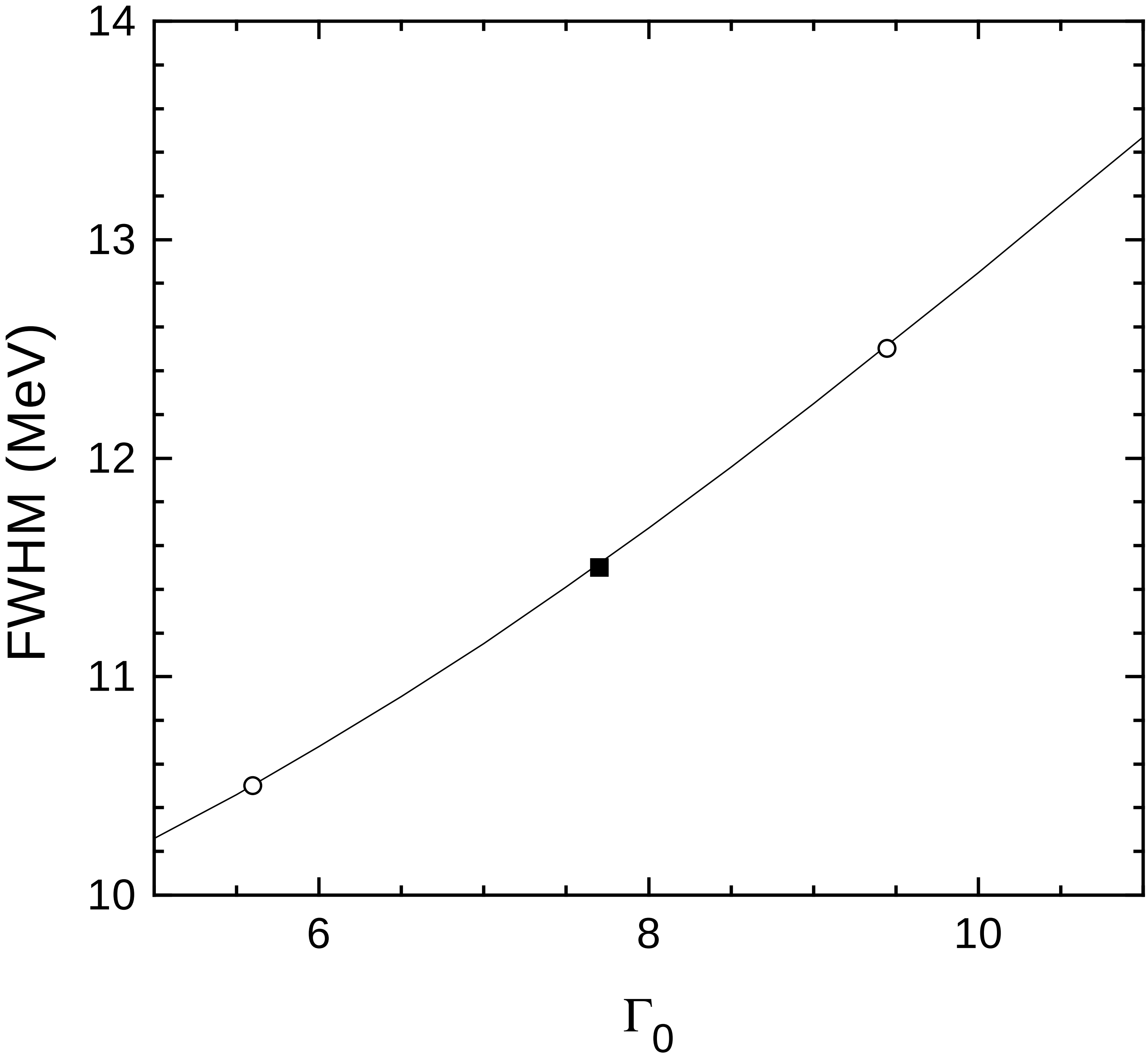

14
13
12
11
10
FWHM (MeV)
6
8
10
Γ_0

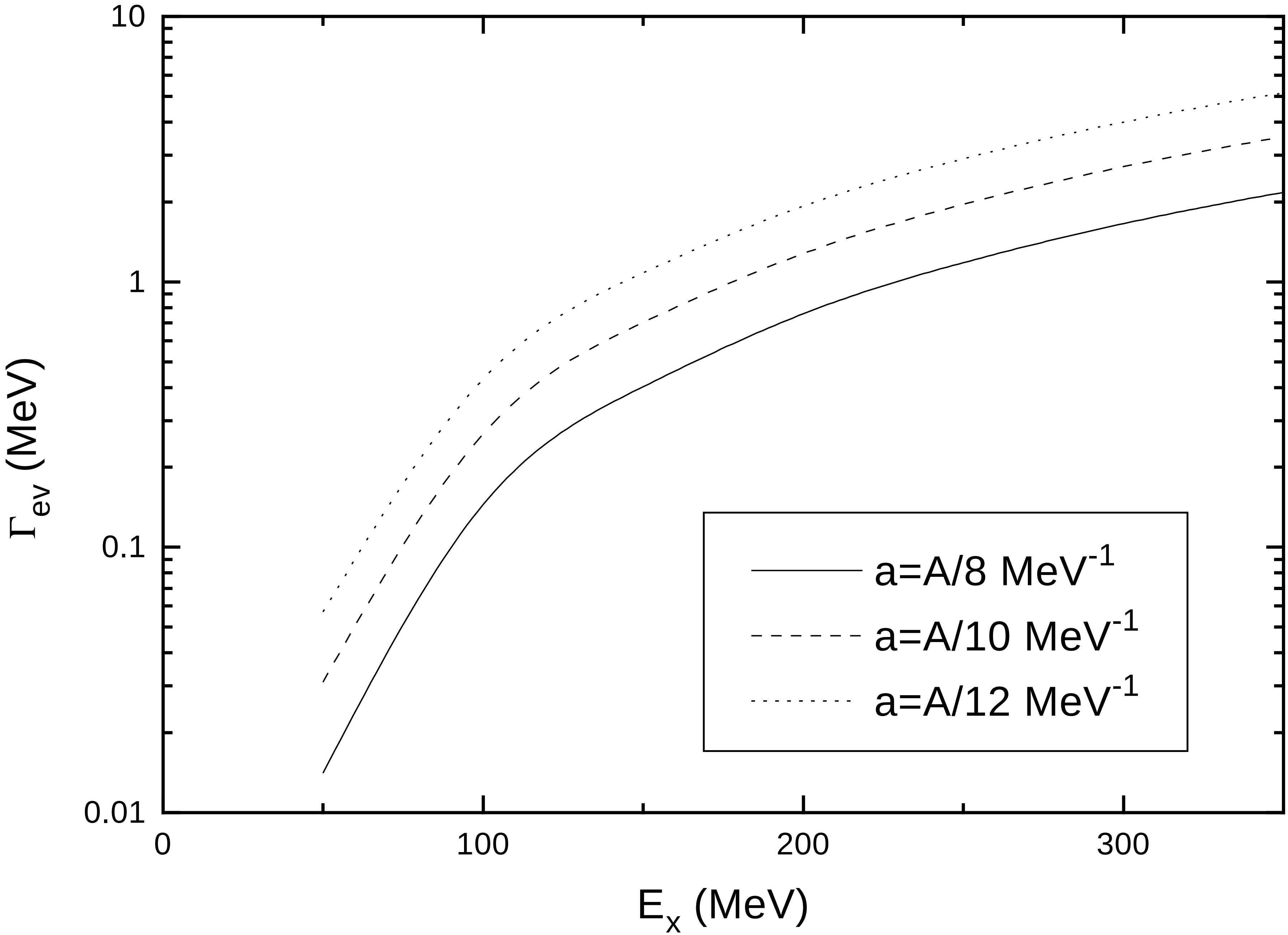

10
1
0.1
0.01
0
100
200
300
Γ_{ev} (MeV)
E_x (MeV)
a=A/8 MeV^{-1}
a=A/10 MeV^{-1}
a=A/12 MeV^{-1}